Detecting irrigation signals from SMAP L3 and L4 soil moisture: A case study in California's Central Valley

Xin Huang[1], Qing He[1], Naota Hanasaki[1,2], Rolf H. Reichle[3], Taikan Oki[1]

[1]Department of Civil Engineering, The University of Tokyo, Tokyo, Japan

5   [2]Center of Climate Change Adaptation, National Institute for Environmental Studies, Tsukuba, Japan

[3]Global Modeling and Assimilation Office, NASA Goddard Space Flight Center, Greenbelt, MD, USA

Correspondence to: Qing He (heqing@g.ecc.u-tokyo.ac.jp) and Xin Huang (xhuangut@gmail.com)

Abstract: Recent advances in satellite-based soil moisture observations present a promising opportunity to monitor irrigation dynamics from space and support the refinement of hydrological and land surface model simulations. This study presents an

10   approach for identifying irrigation signals using data from the Soil Moisture Active and Passive (SMAP) mission, with feasibility demonstrated in Central Valley, California. The approach leverages two SMAP products: the Level 3 Enhanced product, which provides satellite-based soil moisture observations that inherently capture irrigation effects, and the Level 4 data assimilation product, which incorporates only anomalies from SMAP Level 1 brightness temperature data, thereby excluding irrigation effects. The approach is based on the hypothesis that, after correcting for systematic differences not related

15   to irrigation, the soil moisture difference between the Level 3 and 4 products during the cropping season is primarily attributable to irrigation. This hypothesis is first verified by evaluating soil moisture consistency (i.e., temporal variability and long-term mean values) between the two products. For grid cells that meet this criterion, the mean difference (*MD*) between the two soil moisture products is calculated, separately for the cropping and non-cropping seasons, and then the irrigation signal is identified as the difference in *MD* between the cropping and non-cropping seasons. Validation of the estimated

20   irrigation signal is made by comparing with two benchmark irrigation maps. The results show reasonable spatial correlations between our estimate and the two benchmark maps, with Pearson's correlation coefficients of 0.66 and 0.50, respectively. Findings demonstrate the potential of using SMAP products to extract irrigation effects in regions that have limited precipitation during the cropping season. Compared to other satellite-based irrigation detection studies, the proposed method requires minimal additional data and avoids additional model tuning beyond the SMAP processing.

25   ## 1 Introduction

Irrigated agriculture plays a critical role in meeting global food demands, contributing approximately 40% of the world's agricultural products (FAO and UN Water, 2021). Despite covering only 2% of the Earth's land area, it accounts for nearly 90% of global water consumption (McDermid et al., 2023; Ritchie and Roser, 2018). However, detailed information on the spatio-

temporal distribution of irrigation water use at the global scale remains largely unavailable. Although some studies have

30 attempted to estimate the irrigation water use (Guillaumot et al., 2022; McDermid et al., 2023; Wada et al., 2013), the absence

of continuous, large-scale in-situ measurements hampers both validation and accurate estimation (Hanasaki et al., 2008; Müller

Schmied et al., 2021; Sutanudjaja et al., 2018). Currently, only limited regional in-situ measurements are available (Hanasaki

et al., 2022), and these datasets provide neither long records nor sufficient spatial coverage for large-scale estimation. This

limited validation capability challenges estimation accuracy and underscores the urgent need for the development of large-

35 scale irrigation monitoring datasets. Yet, factors such as the high cost and limited availability of monitoring equipment and the

variability of irrigation practices (See et al., 2023) make it challenging to obtain continuous, large-scale, in-situ irrigation

monitoring data at the global scale (Condon et al., 2021; Ozdogan et al., 2010).

In contrast to in-situ measurement networks, satellite observations provide a promising alternative for irrigation monitoring

(Dorigo et al., 2021; Zhang et al., 2022). With obvious advantages in extensive spatial coverage, continuous time series, and

40 compatibility with grid-based hydrological models (Alfieri et al., 2022), satellite observations offer a unique and convenient

tool for monitoring key state variables related to irrigation, such as soil moisture and evapotranspiration (Foster et al., 2020;

Ihuoma et al., 2021).

Satellite-based irrigation monitoring generally follows one of two main approaches. The first approach is the

evapotranspiration-based method, which assimilates remotely sensed evapotranspiration data into hydrological and energy

45 balance models. This method compares evapotranspiration under conditions without any irrigation inputs to the total

evapotranspiration observed, thereby separating evapotranspiration into precipitation-caused and irrigation-caused parts,

allowing for the estimation of irrigation water (Gowda et al., 2008; Santos et al., 2008). This method has been successfully

applied in some areas such as southern Spain (Droogers et al., 2010), northwest China (Ma et al., 2018), and the Indus basin

(Bastiaanssen et al., 2012). However, the retrieval of evapotranspiration products from multispectral sensors is often limited

50 by weather conditions (Zhang et al., 2016), especially cloud coverage, and by the heavy reliance on hydrological modeling,

which demands extensive ancillary data. Therefore, evapotranspiration products are subject to considerable errors and gaps in

spatial and temporal coverage.

The second approach for satellite-based irrigation monitoring focuses directly on the core variable that is most relevant to

irrigation: soil moisture. Unlike evapotranspiration monitoring, satellite soil moisture observations are primarily derived from

55 microwave radiometers that operate independently of weather conditions. Since soil emissivity is closely linked to soil

moisture, increased moisture results in more pronounced absorption and scattering of microwaves by the soil. Consequently,

microwave radiometers are highly sensitive to soil moisture variations (Njoku and Entekhabi, 1996). Major satellite soil

moisture products include those from the Soil Moisture Active Passive (SMAP) mission (Entekhabi et al., 2010) and the Soil

Moisture and Ocean Salinity (SMOS) mission (Barre et al., 2008). The basic principle for this soil moisture-based method is

60   taking the difference between two soil moisture time series with irrigation effects (usually from satellite products) and without

irrigation effects (usually from model simulations without considering irrigation events) (Brocca et al., 2018).

The key to the soil moisture-based irrigation monitoring approach is to ensure that the time series with and without irrigation

effects are climatologically consistent. Specifically, during the non-cropping season or at non-irrigated grid cells, the model-

simulated soil moisture should be consistent with satellite data in terms of its temporal variability and long-term mean. Several

65   recent studies have successfully applied this approach but require complex model tuning (Jalilvand et al., 2021; Soylu and

Bras, 2024). Several other studies, however, also demonstrate the possibility to avoid such complex model tuning, although

these approaches may exhibit limitations in maintaining climatological consistency. For example, Zaussinger et al. (2019) used

MERRA-2 reanalysis soil moisture data as the soil moisture without irrigation effects, and calculated the difference between

several satellite soil moisture products such as SMAP, AMSR2, and ASCAT to estimate irrigation water use amount. However,

70   because the spatiotemporal statistics of MERRA-2 soil moisture are different from any of the satellite products, the identified

irrigation events as well as the estimated irrigation water amount are subject to considerable risk of biases. On the other hand,

in an algorithm where only one satellite product is used, Lawston et al. (2017) compared the soil moisture time series of two

neighboring grid cells with and without irrigation effects, with the irrigation information known a priori, and took the difference

between these two attributed to irrigation. While this method ensures the climatological consistency of the data, the grid cell-

75   by-grid cell comparisons may make the approach too labor intensive for applications across larger domains.

To address these limitations, the present study attempts to extend the spatial applicability of satellite products to detect

irrigation effects without the need for additional model tuning beyond the standard SMAP processing and without sacrificing

the climatological consistency of the data. To achieve this goal, we take advantage of the different processing levels of SMAP

products, i.e., the Level 3–SMAP Enhanced L3 Radiometer Global and Polar Grid Daily 9 km EASE-Grid Soil Moisture

80   (SMAP L3_E) (ONeill et al., 2023), and the Level 4–SMAP L4 Global 3-hourly 9 km EASE-Grid Surface and Root Zone Soil

Moisture Geophysical Data (SMAP L4) (Reichle et al., 2022). SMAP L3_E provides near-real-time soil moisture observations

derived directly from microwave radiometer measurements; therefore, the irrigation contributions are embedded in its soil

moisture time series when such practices occur in the real world. In contrast, SMAP L4 assimilates only time series anomaly

information from the SMAP Level 1 brightness temperature (T_b) observations into the Catchment Land Surface Model (Koster

85   et al., 2000), which provides two major advantages here: (1) Since only anomalies of T_b are assimilated, SMAP L4 does not

contain irrigation effects (as further explained in Section 2.1.2); and (2) the SMAP L3_E and L4 algorithms use nearly identical

microwave radiative transfer models, thereby minimizing the systematic differences between the soil moisture estimates from

the two products.

To demonstrate the applicability of our method, we chose the Central Valley in California, USA, one of the most heavily

90   irrigated regions in the world, as the primary study area, and analyzed SMAP L3_E and L4 data from 2016 to 2022. We also examined several heavily irrigated regions elsewhere in the contiguous United States (CONUS) to further evaluate the performance and applicability of the proposed method. Existing studies, including a map of irrigated areas and estimates of irrigation water use, were used here for validation. Compared to previous studies, the primary innovation of the present study is in achieving climatological consistency between the datasets and effectively monitoring irrigation effects without additional

95   model tuning beyond the SMAP processing.

The paper is organized as follows. Section 2 provides a brief introduction to the data and study area. Section 3 details the methodologies for identifying irrigation signals. Section 4 presents the case study and results, and Sections 5 and 6 offer the discussion and conclusions, respectively.

2 Data and study area

100   ### 2.1 Data

Since its launch in 2015, SMAP has been instrumental in monitoring global soil moisture and freeze-thaw dynamics (Colliander et al., 2022; Fang et al., 2019; Jonard et al., 2022; Purdy et al., 2018; Melser et al., 2024). The satellite is equipped with an L-band passive microwave radiometer. L-band microwave emission from the soil is capable of penetrating clouds and modest amounts of vegetation. Consequently, these T_b observations can be used to retrieve soil moisture estimates by applying a zero-

105   order ("tau-omega") microwave radiative transfer model (Njoku and Entekhabi, 1996), yielding global estimates of soil moisture with 2-3 day revisit frequency (depending on latitude). The present study focuses on the SMAP L3_E and L4 products, which are both provided on the 9 km Equal-Area Scalable Earth (EASE) Grid 2.0. The analysis spans the temporal period from January 1, 2016 to December 31, 2022. SMAP products are available through the National Aeronautics and Space Administration (NASA) Earthdata website (https://earthdata.nasa.gov/, last accessed on October 13, 2024).

110   This study employs SMAP L4, which excludes irrigation effects, as a model-simulated soil moisture reference, and SMAP L3_E as a satellite-observed soil moisture reference that captures irrigation effects. By analyzing the discrepancies between the two, we aim to identify potential irrigation signals.

2.1.1 SMAP L3_E

Surface soil moisture estimates from the SMAP L3_E product were used. Limited by the soil penetration depth of L-band

115 microwaves, the nominal detection depth of this product is 5 cm. Nevertheless, surface soil moisture is often representative of

moisture conditions in deeper layers (Feldman et al., 2023). Compared to soil moisture in the root zone or the full soil profile,

surface soil moisture is particularly sensitive to irrigation activities because irrigation directly alters the moisture content within

this layer.

The L3_E product is a daily composite of SMAP Level 2 half-orbit soil moisture data, which are retrieved from SMAP Level

120 1 T_b data. Although Backus-Gilbert optimal interpolation is applied to post the original 36 km data onto the 9 km EASE Grid

2.0, we note that the relatively coarse effective resolution (closer to 33 km) means that some irrigation features will not be

seen clearly by SMAP. We will further discuss this in Section 4.

SMAP L3_E is categorized into two groups: AM group, collected during the descending pass of the satellite at 06:00 local

solar time, and PM group, collected during the ascending pass at 18:00 local solar time (ONeill et al., 2023). Since the SMAP

125 soil moisture retrieval algorithm requires ancillary soil temperature inputs, here we use the AM soil moisture retrievals because

in the morning the temperature is typically similar across the soil, vegetation, and near-surface air, and the resulting retrievals

are therefore expected to be of higher quality.

2.1.2 SMAP L4 and explanation for the absence of irrigation effects

(1) SMAP L4

130 SMAP L4 is a model-derived product generated using the Catchment land surface model. It utilizes an ensemble Kalman filter

(EnKF) data assimilation system (Reichle et al., 2017b). This system integrates (temporal) anomalies of SMAP Level 1 T_b

observations and provides a comprehensive global soil moisture product that includes the surface layer, the root zone (defined

as 0–1 m depth), and the full soil profile, with complete spatial and temporal coverage (Reichle et al., 2019). Since the SMAP

L3_E product provides only surface soil moisture, we use only surface soil moisture from the SMAP L4 product.

135 SMAP L4 provides global observations every 3 hours on the 9 km EASE-Grid 2.0. Here, arithmetic averaging was applied to

the 3-hourly data to derive daily values, and the resulting daily SMAP L4 values were cross-masked to match the approximately

2–3-day revisiting frequency of SMAP L3_E to enable a more straightforward comparison.

(2) Explanation for the absence of irrigation effects in SMAP L4

The assimilation process of SMAP L4 incorporates only the anomaly time series from the SMAP Level 1 T_b product. A mean

140 seasonal cycle of T_b is calculated separately for the Level 1 T_b observations and the corresponding model estimates, where the

mean seasonal cycle is computed as the multi-year mean for a given day of year, with roughly monthly smoothing. Observed

anomalies are then calculated by subtracting the mean seasonal cycle from the original T_b time series of SMAP Level 1

observations; anomalies for the corresponding model estimates are calculated in the same fashion (Reichle et al., 2017a; De Lannoy and Reichle, 2016). In irrigated regions, where crop area, cultivation type, and irrigation requirements remain relatively

145 stable over several years, the SMAP Level 1 T_b product reflects the impact of irrigation on soil moisture levels as part of the monthly seasonal mean, rather than classifying it as an increased anomaly. Consequently, the T_b anomaly time series assimilated in SMAP L4 inherently excludes irrigation effects, leading to the absence of irrigation effects in the SMAP L4 product.

2.1.3 Supporting data

150 (1) Precipitation

Precipitation is obtained from the Catchment model forcing dataset released with SMAP L4. Over CONUS, this dataset primarily sources its information from NOAA Climate Prediction Center Unified gauge-based precipitation data. A detailed description is available in Reichle et al. (2023). The precipitation data can help understand the variability of SMAP L3_E and L4 and distinguish whether the differences between two soil moisture products are driven by precipitation or by other factors,

155 such as irrigation.

(2) Map of irrigated area

This study utilized the latest Global Map of Irrigated Area (GMIA) provided by the Food and Agriculture Organization (FAO) of the United Nations. The GMIA is a static dataset that represents the percentage of irrigated land relative to the total grid cell area around 2005 (Siebert et al., 2013). It offers global coverage at a 5 arcmin resolution and was resampled to the 9 km EASE-

160 Grid 2.0 using nearest-neighbor interpolation for comparative analysis.

GMIA is used to identify non-irrigated grid cells and those with varying irrigation fractions. It serves both as the basis for examining consistency in Section 3.1 and as a validation source for proposed irrigation signals analysis in Section 3.2.

(3) Irrigation water use estimation

To further validate our approach, we compared the derived irrigation signal map with independent irrigation water use

165 estimations. Currently, large-scale in-situ irrigation water use measurements are hardly available. Although USGS provides state-level data (e.g., 2000, 2005, 2010, 2015) and USDA offers county-level survey data (e.g., 2003, 2008, 2013, 2018), only the 2018 dataset overlaps with the SMAP observation period. Moreover, the broader spatial aggregation and lower temporal resolution of these datasets limit their applicability for direct comparison.

To address these limitations, we selected the estimated irrigation water use map provided by Zhang and Long (2021), hereafter

170 referred to as the ZL21 map. Derived from model simulations that integrate remote sensing-based evapotranspiration with simulated root zone soil moisture, the ZL21 map offers high-resolution (1 km) monthly irrigation water use estimates for the CONUS over the period 2000–2020. For the comparison, the ZL21 map was resampled to a 9 km EASE-Grid 2.0 and the monthly data were aggregated to obtain the total irrigation water use during the cropping season. This dataset permits a more direct and accurate large-scale comparison with our proposed irrigation signal map than the coarser state-level and county-

175 level data.

2.2 Study area

According to the validation reports for the SMAP Level 2/Level 3 product (O'Neill et al., 2020) and the SMAP L4 product (Reichle et al., 2023a), these products are supported by the most extensive network of validation sites in CONUS, where their accuracy is considered to be greatest. Given these considerations, the present study selected the Central Valley in California,

180 one of the largest irrigation regions in the world, as the primary study area. Additionally, experiments were conducted in Snake River Plain and Nebraska High Plains to evaluate the broader applicability of the proposed method. Figures 1a and 1b illustrate the geographical location and the map of irrigated areas of Central Valley and CONUS.
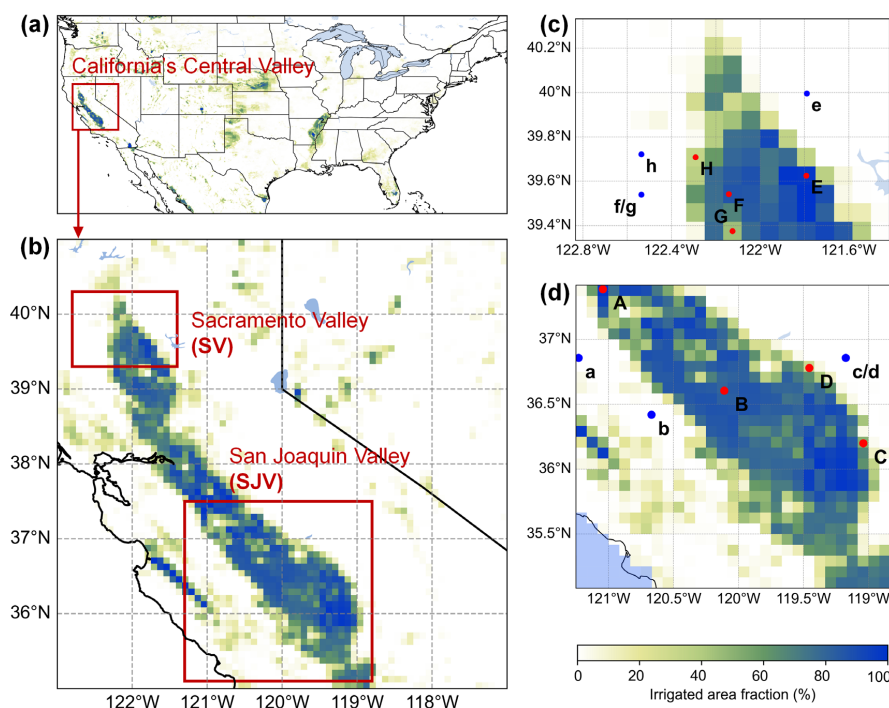

Figure 1: Geographical locations of (a) CONUS, (b) California's Central Valley, (c) Sacramento Valley, and (d) San Joaquin Valley.

185 **Shading illustrates irrigated area fraction from GMIA. Blue circles and lower-case letters in (c) and (d) denote non-irrigated grid cells; red circles and upper-case letters represent irrigated grid cells; and light blue areas in (d) denote grid cells located over the ocean.**

The United States National Agricultural Statistics Service identifies the Central Valley as the most irrigation-intensive region in CONUS, accounting for approximately 16% of the national total irrigation water usage (U.S. Department of Agriculture, 2024). Moreover, the Central Valley features different climate zones (Yang et al., 2017) and irrigation technologies, making it an ideal location to assess the performance of the proposed method under different conditions.

This study further divided the Central Valley into two subregions based on differing climate and irrigation practices: the southern San Joaquin Valley (SJV), which features a semi-arid climate and is predominantly equipped with sprinkler systems, and the northern Sacramento Valley (SV), characterized by a Mediterranean climate (Kottek et al., 2006) and primarily featuring flood irrigation systems. The main crops in SJV include almonds, grapes, and cotton, whereas rice dominates SV's farmlands. In fact, SV accounts for 95% of California's rice production and approximately 20% of the total rice production in CONUS (Singh et al., 2017). Given the high water demand of rice cultivation, SV relies more heavily on irrigation. In this region, rice farmlands are saturated from late April or early May, with planting commencing shortly thereafter, and they remain saturated with irrigation water until early September, when the farmlands are drained for harvest (Lawston et al., 2017).

3 Methodology

Identifying irrigation signals from SMAP L3_E and SMAP L4 is based on the assumption that the soil moisture difference between the two products stems from human irrigation activities under the following conditions: (1) the signal must be observed during the cropping season, (2) the bias between SMAP L3_E and L4 remains consistent across the cropping and non-cropping seasons, and (3) SMAP L3_E is significantly higher than L4. Note that these conditions allow for the presence of bias between SMAP L3_E and L4, as long as the bias remains consistent across the cropping and non-cropping seasons, which can be assessed in nearby grid cells that have no irrigation.

3.1 Evaluating the consistency between SMAP L3_E and L4

This section outlines how we evaluate the consistency between the SMAP L3_E and L4 products to ensure that the irrigation signal is genuine and not merely an artifact of systematic error in the L3_E and/or L4 product. This was accomplished by applying two criteria (described in the following paragraphs) to non-irrigated grid cells. The independent irrigated area map (GMIA) was used to locate the non-irrigated grid cells (defined as those with an irrigated area fraction below 0.1%). To reduce the sample size and improve clarity, a subsampling procedure was performed on these non-irrigated grid cells, involving two steps: (1) selection of all non-irrigated land grid cells as initially defined, and (2) uniform subsampling of these grid cells with a fixed interval. It is noted that this subsampling step is performed solely for clarity of presentation and does not influence the integrity or the overall analysis. Additionally, the crop calendar developed by Sacks et al. (2010) was employed to delineate

the cropping and non-cropping seasons.

The two criteria used to evaluate the consistency of two soil moisture products during the cropping and non-cropping seasons are as follows: The first criterion is the Pearson correlation coefficient R across the entire period between the SMAP L3_E and L4 time series, which assesses the consistency in terms of the time series variability. A high R value indicates that both products

220 exhibit similar variability in soil moisture dynamics and respond similarly to temporal variability in meteorological changes. We calculate R across the entire time period and assume that the two products have consistent variability when $R > 0.70$. (Sensitivity analysis results for other thresholds, including 0.50, 0.60, and 0.80, are detailed in Supplementary Information Section S1.)

The second criterion is based on the Mean Difference (MD) between the SMAP L3_E and L4 data:

$$MD = \frac{1}{n}\sum_{i=1}^{n}(\theta_{L3,i} - \theta_{L4,i}) \qquad (1)$$

where n is the number of soil moisture samples (dimensionless) and $\theta_{L3,i}$ and $\theta_{L4,i}$ are the soil moisture values at time i from SMAP L3_E and L4, respectively (m^3/m^3). We calculate MD values for the cropping and non-cropping seasons individually in non-irrigated grid cells, and then compare the MD values to assess whether the bias is consistent across both seasons. When the MD values for the two seasons are within ± 0.04 m^3/m^3, we assume that the mean soil moisture difference between the

230 two products is consistent across the two seasons and therefore largely unaffected by systematic error between the SMAP L3_E retrieval algorithm and the physical parameterizations of the L4 land surface model. The ± 0.04 m^3/m^3 threshold for MD consistency used here equals the unbiased Root Mean Square Error ($ubRMSE$) accuracy requirement of SMAP soil moisture products. When the MD values are within ± 0.04 m^3/m^3, the SMAP L3_E and L4 soil moisture are considered to be climatologically consistent across the cropping and non-cropping seasons in non-irrigated grid cells.

235 Next, we hypothesize that the soil moisture climatology is consistent among irrigated and non-irrigated grid cells within the study area. That is, if non-irrigated grid cells exhibit consistent seasonal bias across the cropping and non-cropping seasons, a similar consistency is assumed for irrigated grid cells.

3.2 Identification of SMAP's irrigation signals

After confirming the consistency of SMAP L3_E and L4 at non-irrigated grid cells, the irrigation signals can be identified as

240 the difference in the MD between the cropping and non-cropping seasons. Quantitatively, we define the Irrigation Signal (IS), separately for each grid cell, as the difference between the MD values during the cropping and non-cropping seasons:

$$IS = MD_{cro} - MD_{non} \tag{2}$$

where MD_{cro} and MD_{non} denote the L3_E-minus-L4 mean difference for the same grid cell during cropping and non-cropping seasons, respectively (m³/m³). A larger IS value indicates a higher irrigation intensity for the grid cell. Note that IS represents

245   irrigation intensity rather than the absolute irrigation water use amount; this distinction is further elaborated in Section 5.

We applied the quantitative IS method across the entire study area to map irrigation intensity, excluding the grid cells that do not meet the climatological consistency criteria. Recall that for the consistency evaluation in non-irrigated grid cells, we compute R across the entire year. For the IS map, however, we calculated R only during the non-cropping season (R_{non}) because irrigation during the cropping season is expected to elevate soil moisture in irrigated grid cells, which is captured in SMAP

250   L3_E but not in L4. To validate our results, the multi-year average IS map is compared with both the GMIA map and the ZL21 map.

4 Results

4.1 Verification of SMAP L3_E and L4 data consistency

To verify climatological consistency between SMAP L3_E and L4 across the cropping and non-cropping seasons, soil moisture

255   estimates of non-irrigated grid cells from 2016 to 2022 were analyzed. Within the SJV and SV regions, a total of 32 grid cells were subsampled from the pool of non-irrigated grid cells (irrigated area fraction below 0.1%) to ensure representative coverage (Supplementary Information Section S2). For brevity, only six selected grid cells are shown in the main text. Figure 1c, 1d, and Table 1 display the locations of these non-irrigated grid cells (blue circles) along with their irrigated area fractions as reported by the GMIA.

260   For further comparison in the next section, the corresponding irrigated grid cells (red circles) of each selected non-irrigated sample are presented. These grid cells were selected by two criteria: (1) geographic proximity to the sampled non-irrigated grid cells and (2) irrigation fractions that closely match target fractions—near 100%, 80%, 50%, and 30% as reported by the GMIA. In cases where multiple irrigated grid cells were in very close proximity (e.g., grid cells C and D; or F and G), they were paired with the same non-irrigated grid cell (e.g., grid cells c/d; or f/g). Additionally, as a sensitivity test, 10 alternative

265   pairs were analyzed (see Supplementary Information Section S3) to verify the robustness of our hypothesis.

Table 1: Irrigated area fractions from GMIA for selected non-irrigated and irrigated grid cells

Region	Non-irrigated grid cells		Irrigated grid cells	
	Grid cell No.	Irrigated area fraction	Grid cell No.	Irrigated area fraction
SJV	a	0.00%	A	99.70%
	b	0.11%	B	80.02%
	c/d	0.00%	C	50.79%
			D	30.20%
SV	e	0.00%	E	92.11%
	f/g	0.00%	F	81.05%
			G	42.14%
	h	0.00%	H	30.97%

Figure 2 displays the soil moisture time series from SMAP L3_E and L4 for the six selected non-irrigated grid cells in 2016. The cropping season (May to October) and the non-cropping season (November to April) are defined based on crop calendars from Sacks et al. (2010). Visual inspection indicates that the temporal variabilities of SMAP L3_E and L4 correspond reasonably well throughout the year. Specifically, both retrievals exhibit high variability during the non-cropping season when a considerable amount of precipitation occurs, while dropping to a low, quasi-constant level during the cropping season when precipitation is scarce.

A quantitative evaluation using R and MD suggests that SMAP L3_E and L4 are systematically consistent in the Central Valley. In all selected non-irrigated grid cells, R exceeds 0.70 and the difference between the cropping season MD (MD_{cro}) and the non-cropping season MD (MD_{non}) remains within ± 0.04 m³/m³. (Time series of differences between SMAP L3_E and L4 in non-irrigated grid cells are provided in the Supplementary Information Figure S4-1.) As detailed in the Supplementary Information Section S2, 93.8% (30 out of 32) sampled non-irrigated grid cells meet these criteria. Furthermore, a paired t-test showed no statistically significant difference between MD_{non} and MD_{cro} (p-value > 0.05), indicating that SMAP L3_E and L4 exhibit similar responses to the temporal variability and maintain a consistent bias across the cropping and non-cropping seasons.
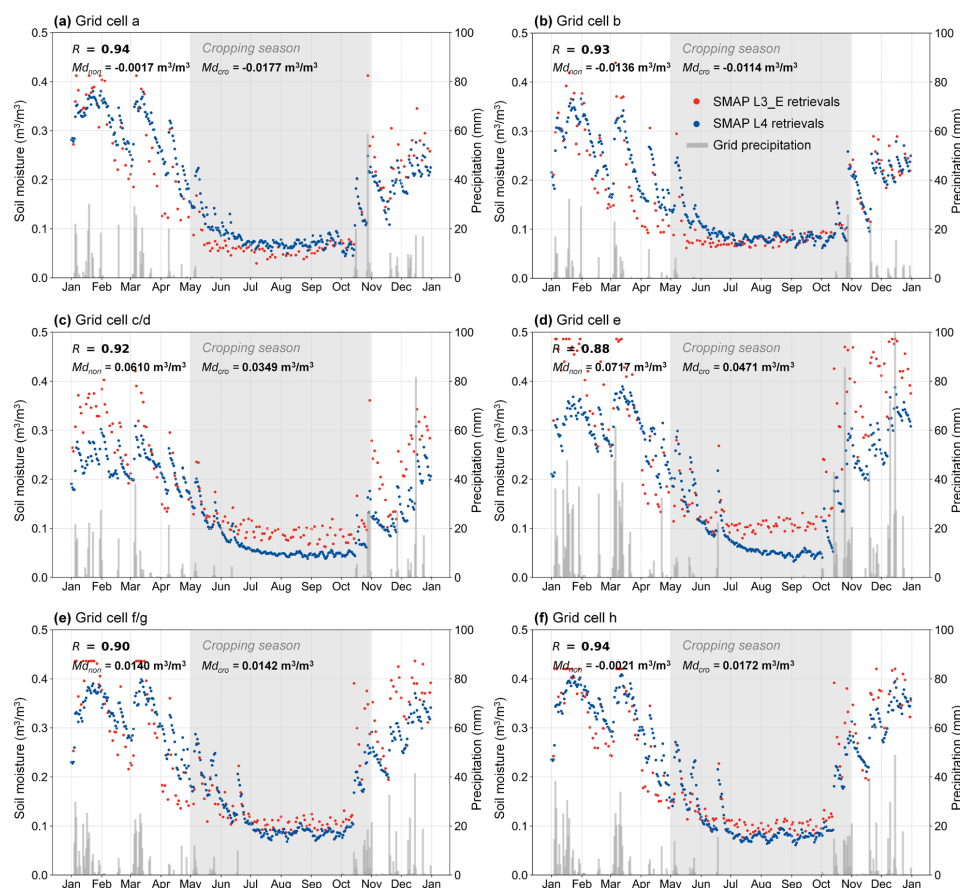
Figure 2: SMAP surface soil moisture from (red dots) L3_E and (blue dots) L4 for selected non-irrigated grid cells in 2016 (left axis). Gray bars indicate precipitation (right axis), and light gray shaded area represents the cropping season. See Figure 1 for grid cell locations.

4.2 Verification of detected irrigation signals at the point scale

4.2.1 San Joaquin Valley

Figure 3 presents the SMAP L3_E and L4 soil moisture for four irrigated grid cells in SJV in 2016. The temporal variability of the two products is climatologically consistent during the non-cropping season, with Pearson correlation coefficient R_{non} exceeding 0.70. Supplementary Information Figure S5-3 reinforces this observation, which shows that 100% (18 out of 18) uniformly sampled irrigated grid cells have R_{non} values above 0.70, confirming the consistency of both products. At the same time, both visual inspection and statistical analysis indicate that, while the two soil moisture time series are similar during the non-cropping season, a significant gap emerges during the cropping season. Specifically, MD_{cro} is much higher than MD_{non}, a difference confirmed as statistically significant by a paired t-test (detailed in the following paragraph). In the absence of

precipitation during the cropping season, the higher soil moisture level in SMAP L3_E suggests that the additional soil water

is likely owing to human irrigation activities.
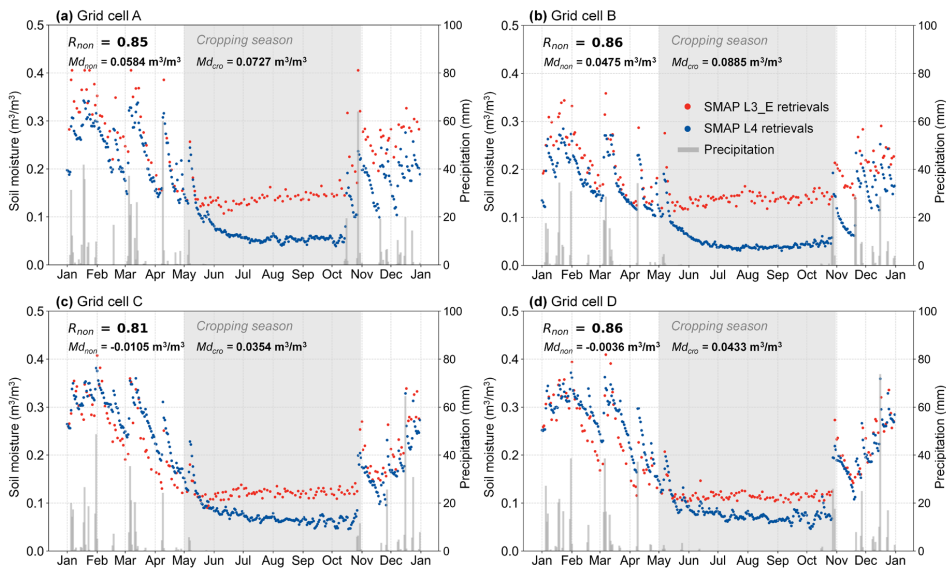
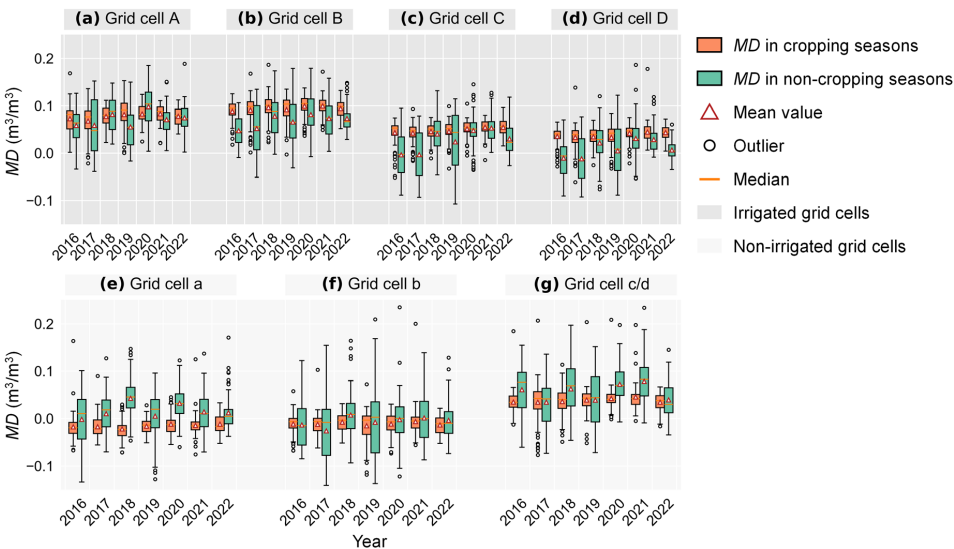Figure 3: As in Figure 2 but for selected irrigated grid cells in SJV, 2016.

Figure 4: Distribution of *MD* values in the (red) cropping and (green) non-cropping seasons for selected (top row) irrigated and

(bottom row) non-irrigated grid cells in SJV from 2016 to 2022. See Figure 1 for grid cell locations.

305   To quantitatively demonstrate the presence of irrigation signals at these grid cells, we compared MD of the SMAP L3_E and
L4 between the cropping and non-cropping seasons in SJV from 2016 to 2022 (Fig. 4). A paired t-test was conducted to assess
whether the MD values differ significantly between the two seasons (time series of differences between SMAP L3_E and L4
in selected irrigated grid cells are provided in the Supplementary Information Figure S4-2). At the irrigated grid cells (Figs.
4a–d), we generally observed higher MD values during the cropping season compared to those during non-cropping season (p-

310   value < 0.05), although exceptions exist, such as grid cell A in 2020. In contrast, the cropping and non-cropping gaps of MD
at the non-irrigated grid cells (Figs. 4e–g) are close enough to be neglected: the MD difference between the two seasons are
generally within ± 0.04 m³/m³. The paired t-test results (p-value = 0.2056 > 0.05) reinforce that there is no statistically
significant difference of the MD values between the two seasons. Together, these results quantitatively demonstrate that our
identification method is valid, indicating that the significant soil moisture gaps during the cropping season at irrigated grid

315   cells are likely due to irrigation rather than other systematic differences between the two SMAP products.

4.2.2 Sacramento Valley

Figure 5 presents the SMAP L3_E and L4 soil moisture for four irrigated grid cells in SV in 2016. In contrast to the results for
SJV, we observed that not all regions in the Central Valley exhibit high climatological consistency between SMAP L3_E and
L4. For example, the three selected irrigated grid cells in SV (Figs. 5a-c and 6a–c) show inconsistent variability during the

320   non-cropping season (R_{non} < 0.70). In Supplementary Information Figure S5-3, we show that 72.7% (8 out of 11) uniformly
sampled irrigated grid cells in SV have R_{non} below this threshold. This decrease in R_{non} is attributed to the SMAP L3_E
algorithm producing several saturated soil moisture points (Figs. 6a–c, Supplementary Information Figure S2-4) during the
non-cropping season, while SMAP L4, although also indicating high soil moisture levels, remains unsaturated. Note that these
grid cells will be classified as having inconsistent climatology in the subsequent irrigation signal map analysis.
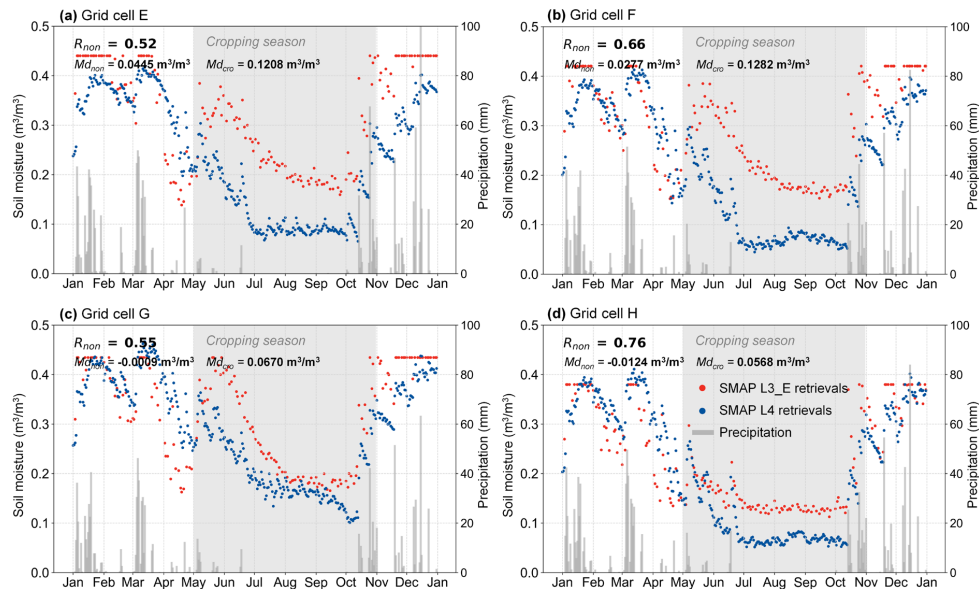
Figure 5: As in Figure 2 but for selected irrigated grid cells in SV, 2016.

Furthermore, Figure 6 compares *MD* between the cropping and non-cropping seasons. A marked increase in *MD* during the cropping season was observed in irrigated grid cells (Figs. 6a–d), with SMAP L3_E soil moisture retrieval showing a more significant increase during the cropping season. This is likely driven by the high irrigation water demand associated with large-scale rice cultivation in SV (Wong et al., 2021).
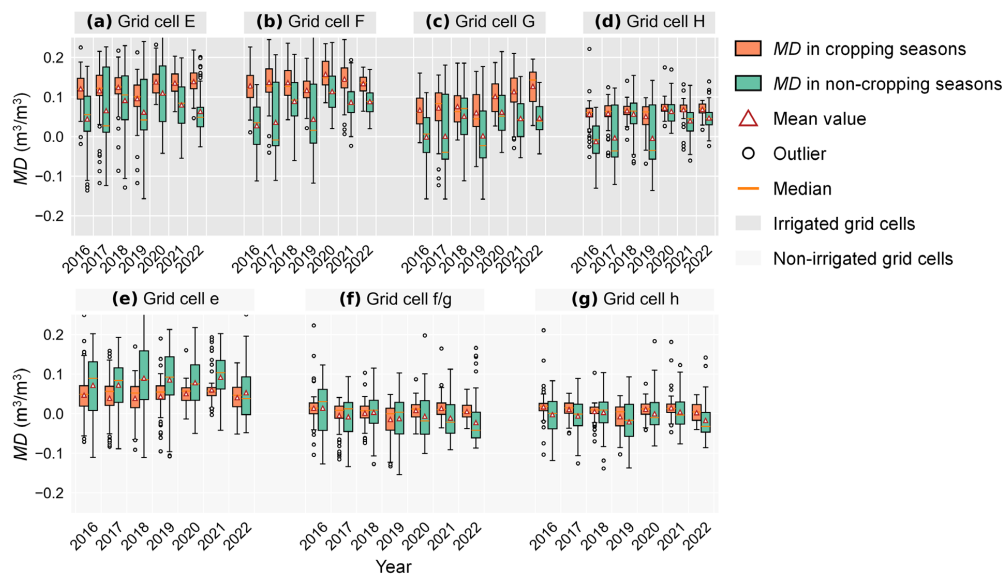

Figure 6: As in Figure 5 but for selected grid cells in SV.

15

4.3 Map of SMAP's irrigation signals in San Joaquin Valley

Having confirmed the climatological consistency between the two satellite products and verified the validity of the irrigation

335   detection method at several point locations, we now present a map of SMAP-based irrigation intensity. Figure 7 shows the

estimated average *IS* for SJV from 2016 to 2020 (Fig. 7a), alongside the corresponding irrigated area fraction from the GMIA

(Fig. 7b) and the average irrigation water use derived from the ZL21 map (Fig. 7c). To maintain conciseness, the estimated *IS*

map for SV is provided in Supplementary Information Section S6. The elliptical irrigation signal shape, extending from

northwest to southeast, can be identified in SJV. In addition, localized irrigation signals are detected in some smaller farmlands,

340   such as the regions (i) Salinas Valley and (ii) most southern part of SJV in Fig. 7, which are also recognized as irrigated in the

GMIA and the ZL21 map. In the northeast of SJV, at the edge of Sierra Nevada mountains (Supplementary Information Figure

S7-1), we observe a small fraction of grid cells where the non-cropping season soil moisture time series is not consistent

(shown in gray shading in Fig. 7a). This inconsistency is attributed to the high elevation in this region, where soil remains

frozen or snow-covered during the non-cropping season (primarily winter and spring). Under such conditions, the microwave

345   radiative transfer model used in the SMAP L3_E retrieval algorithm and the L4 model assimilation cannot properly simulate

the link between soil moisture and brightness temperature. Consequently, the L3_E algorithm flags the retrievals for

questionable quality, and the L4 algorithm does not assimilate the SMAP-observed brightness temperature.
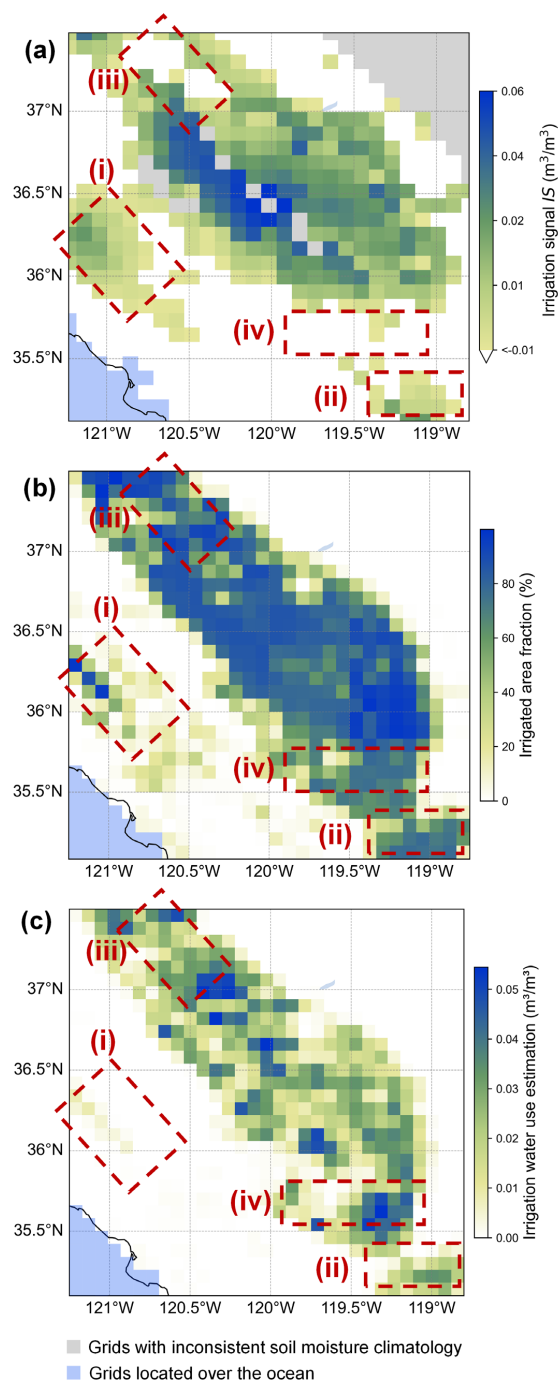
Figure 7: Map of irrigation signals (*IS*) and the validations in SJV. (a) Average *IS* estimated from SMAP for 2016–2020, (b) irrigated area fraction from the GMIA, and (c) average irrigation water use estimations for 2016–2020 from the ZL21 map. Light blue areas

denote grid cells located over the ocean, while gray colored areas indicate grid cells with inconsistent soil moisture climatology. Note: While both the *IS* map and the ZL21 map (e.g., Figs. 7a, 7c) share the same units, they differ in their interpretation. The ZL21 map quantifies irrigation water use per cubic meter, whereas the *IS* map primarily captures the accumulated soil moisture differences

355 **between SMAP L3_E and L4 products, making their absolute magnitudes non-comparable and relevant only in terms of intensity.**

Figure 8 displays the scatterplot and *R* values between the estimated average *IS* map and the irrigated area fraction from the GMIA (Fig. 8a) as well as the average irrigation water use estimations from the ZL21 map (Fig. 8b). Sensitivity analysis scatterplots for different soil moisture variability consistency thresholds are detailed in Supplementary Information Section S8.

360 The scatterplot for two benchmark products irrigated area fraction and average irrigation water use estimations is shown in Fig. 8c. The spatial correlation with the GMIA and ZL21 map are 0.66 and 0.50, respectively. These results further suggest that our proposed method–where only SMAP L3_E and L4 soil moisture are used–is valid and SMAP products do have the potential to reveal irrigation effects.
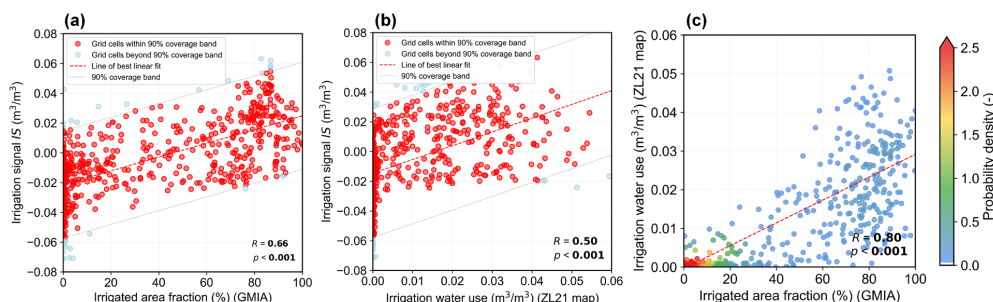

365 **Figure 8: Scatterplot of grid cell values in the *IS* map compared with those from the GMIA and the ZL21 map in SJV. (a) Comparison between the *IS* and irrigated area fraction (GMIA), (b) comparison between the *IS* and the irrigation water use (ZL21 map), and (c) comparison between the two benchmark products: the irrigated water use (GMIA) and the irrigation water use (ZL21 map).**

However, some discrepancies remain between the irrigated area (GMIA), the irrigation water use estimation (ZL21 map), and

370 the proposed *IS* map. First, the spatial gradients in the *IS* map derived from SMAP tend to be smoother, likely due to its effective spatial resolution being coarser than the nominal 9 km EASE-Grid, as the native radiometer footprint (~36 km) is interpolated to the nominal resolution by the Backus-Gilbert optimal interpolation algorithm (ONeill et al., 2023). This smoothing could explain why some grid cells along the boundaries of irrigation regions show near-zero values in the GMIA and ZL21 maps but non-zero values in the *IS* map in Fig. 8. Second, the satellite-based results strongly reflect the local

375 characteristics. For instance, over grid cells in region (iii) (around 37.3°N, 120.7°W), the GMIA indicates high irrigated

fractions, whereas both the ZL21 map and the proposed *IS* map show weak irrigation effects. This discrepancy is probably caused by intensive urbanization in this area, as directly observed on Google Earth (Supplementary Information Section S9); since the GMIA was estimated based on the global irrigated land data in 2005 (Siebert et al., 2013), any subsequent changes are not captured in the GMIA. Nonetheless, limitations also exist in the satellite-based approach. In region (iv) (around 35.6°N,

380   119.5°W), the *IS* map shows little or no irrigation signal, despite both the GMIA and the ZL21 map indicating heavy irrigation. This discrepancy could be due to the prevalence of developed subsurface irrigation systems in this area (Faunt, 2009; Sorooshian et al., 2014). The estimated *IS* map relies solely on satellite-based surface soil moisture so that it cannot monitor the water that transfers directly to the root zone soil.

5 Discussion

385   This study demonstrates the feasibility of detecting irrigation effects from SMAP soil moisture products in the Central Valley. Applying the approach to monitor irrigation water use on a global scale still faces several noteworthy technical challenges. These challenges include ensuring the effectiveness of detection methods across diverse climatic conditions and addressing the limitation of our method, which can identify whether a region is irrigated and estimate relative intensity, but not quantify the exact amount of irrigation water used. In this section, we discuss these issues based on our extended analyses and a review

390   of relevant literature, aiming to provide insights for future large-scale irrigation estimation studies based mainly on satellite-derived soil moisture.

5.1 Evaluation of detection effectiveness across different climatic conditions

Our results indicate that the proposed method based on mean differences between SMAP L3_E and L4 data works reasonably well in revealing irrigation signals in the Central Valley, where dry summer and marginal precipitation during the cropping

395   season make these signals distinct. In such regions with dry summer climates (e.g., (semi-)arid or (semi-)Mediterranean climates), increases in soil moisture containing irrigation effects can be confidently attributed to irrigation activities. However, other regions may experience year-round precipitation or precipitation overlapping with the cropping season. To further evaluate the effectiveness of our method under these conditions, we extended our analysis to two additional irrigation regions in CONUS: the Snake River Plain (SRP) in Idaho, and the Nebraska High Plains (NHP). SRP is characterized by a cold semi-

400   arid climate (Kottek et al., 2006) with marginal precipitation during both the cropping season and summer, and Idaho is the second-largest state in CONUS in terms of irrigation water withdrawals (Murray, 2018). In contrast, NHP lies in a transitional climatic zone: its western part is semi-arid, while its eastern part features a humid continental climate with year-round precipitation (Kottek et al., 2006). The primary crops in NHP are corn and soybean, with irrigation requirements for corn decreasing from approximately 350 mm per year in the western NHP to about 150 mm per year in the eastern NHP (Zaussinger

405 et al., 2019).

Based on our method, we expect the *MD* between two SMAP products to be higher during the cropping season than during the non-cropping season for the irrigated grid cells. In SRP, soil moisture behavior aligns with this expectation, with *MD* significantly higher from June to October (Fig. 9). However, in NHP, the *MD* difference is only marginal due to consistent precipitation throughout the year (Fig. 10). The proposed *IS* maps for SRP and NHP are provided in Supplementary Information

410 Section S10. These results indicate that our method can only effectively capture irrigation signals in regions with limited cropping season precipitation (e.g., (semi-)arid, (semi-)Mediterranean climatic regions). The challenge of precipitation interfering with the detection of irrigation effects in regions where precipitation overlaps with irrigation is not new in satellite-based irrigation detection studies. For example, Lawston et al. (2017) reported clear irrigation effects from SMAP L3 products in Sacramento Valley and San Luis Valley, where (semi-)Mediterranean climates with dry summers and autumns coincide with

415 cropping seasons. However, eastern Nebraska, the same region as we tested in Figure 10, exhibited blurred irrigation effects due to overlapping precipitation. Similarly, Zaussinger et al. (2019) found that their SMAP-based irrigation estimations are weak in precipitation-dominated irrigation regions like the Lower Mississippi Floodplain and NHP.

One potential solution is to explicitly account for the residual influence after precipitation. For example, estimating how much water from precipitation can be retained in the surface soil layer (e.g., applying the precipitation fraction concept as proposed

420 by McColl et al. (2017)) and subtracting it from the soil moisture observations. Integrating evapotranspiration is another promising approach, although it remains challenging due to the limited availability of reliable large-scale observations.
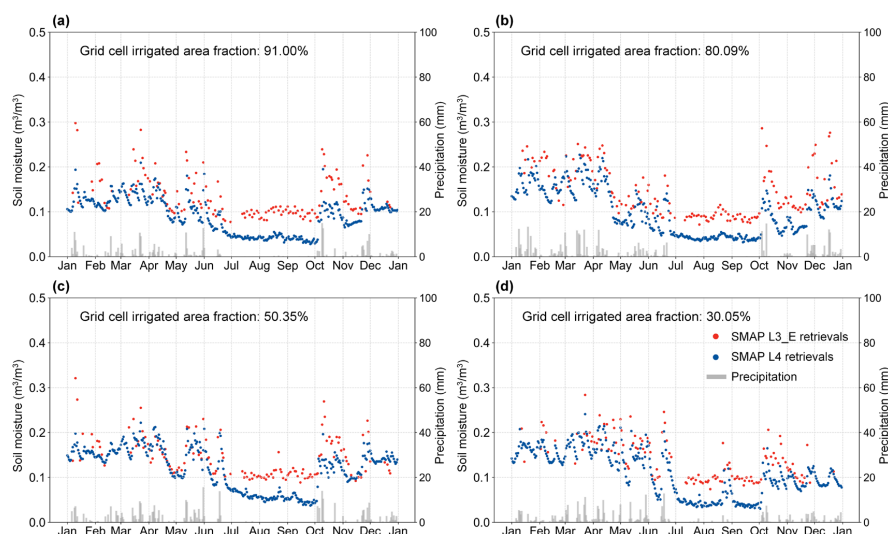

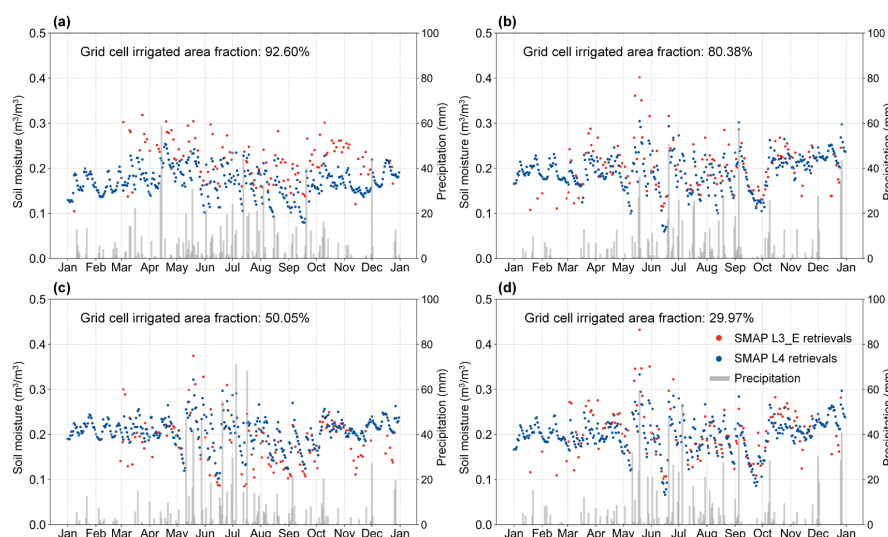Figure 9: As in Figure 2 but for irrigated grid cells in SRP, 2018.

Figure 10: As in Figure 2 but for irrigated grid cells in NHP, 2018.

Grid cells with inconsistent climatology between SMAP L3_E and L4 were masked and excluded from the analysis. In this study, these inconsistencies primarily arise in high-elevation mountainous areas characterized by snow cover, where the temporal variability between the two datasets diverges. Including these grid cells could potentially lead to erroneous interpretations when detecting irrigation signals. Future studies could incorporate additional geographic information, such as elevation and land-use classifications, to better distinguish between irrigated grid cells and high-elevation non-irrigated grid cells, thereby enhancing the reliability of irrigation detection.

5.2 Algorithm complexity for absolute irrigation water amount calculation

Another limitation of this study is that we provide irrigation intensity rather than absolute irrigation water use amounts. This is because satellite-based soil moisture retrievals, such as those from SMAP, represent a stock variable that reflects the integrated effect of various flow processes such as precipitation, evapotranspiration, runoff, and irrigation. In essence, estimating individual components (e.g., irrigation water, runoff, evapotranspiration) of the total flux directly from knowledge of the stock variable is mathematically infeasible. Additionally, factors such as noise, the representativeness of soil depths in satellite retrievals, bias in reference soil moisture data, and the inherent soil moisture memory further complicate the estimation of absolute irrigation water use amounts (Brocca et al., 2018; Foster et al., 2020; Jalilvand et al., 2019, 2023).

To address these challenges, one promising approach is to integrate physical and statistical methods to better characterize the nonlinear soil moisture processes. Specifically, two key water sources should be separated and modeled: (1) precipitation- and

irrigation-caused soil moisture increments and (2) noise and bias versus real soil moisture signals. On the other hand, data-
driven machine learning methods offer a promising alternative to rapidly "learn" intricate relationships between the "true"

445   irrigation water amount and soil moisture (noting that, due to the scarcity of observed data, the "true" amount referenced here
is typically estimated from validated simulation models). This approach has been applied in regional studies as seen in China
(Liu et al., 2024), the state of Kansas (Wei et al., 2022), and other regions. With similar applications extended to other regions,
such maps would provide valuable insights for hydrological modeling and support sustainable water resource management on
a global scale.

450   **6 Conclusions**

In this study, we proposed a method to detect irrigation signals directly from SMAP L3_E and L4 soil moisture products. A
critical foundation of this approach is that SMAP L4 inherently excludes irrigation effects, a key finding confirmed by our
systematic comparison with SMAP Level 3 products. This exclusion arises because SMAP L4 assimilates only brightness
temperature anomalies from SMAP Level 1 observations, where irrigation-induced changes are absorbed into the

455   climatological seasonal mean rather than being treated as anomalies. Our analysis confirms that SMAP L4 soil moisture does
not include irrigation effects, making it a reliable baseline for isolating anthropogenic water use in water resource studies.

By analyzing mean differences during the cropping and non-cropping seasons in Central Valley California, we demonstrate
that SMAP can effectively identify irrigation effects in regions with (semi-)Mediterranean and (semi-)arid climate, where
precipitation during the cropping season is limited. Our application to the Snake River Basin further confirms that the method

460   is effective for regions with similar climatic conditions. However, in regions such as the Nebraska High Plains and the Lower
Mississippi Floodplain, characterized by year-round precipitation or overlapping precipitation and cropping season, the method
struggles to separate irrigation effects from precipitation, rendering it ineffective. We also provide a spatial irrigation signal
map that indicates the irrigation water use intensity. The spatial correlations between our maps and two benchmark maps
demonstrate reasonable agreement, further underscoring the validity of SMAP-based soil moisture retrievals for irrigation

465   monitoring. Compared to other satellite-based irrigation studies that used or developed comprehensive models, our method is
built solely on statistical analyses of two satellite-based pre-tuning soil moisture datasets and shows high simplicity with
minimum requirement of additional data.

One noteworthy limitation of our method is that we cannot explicitly quantify the absolute irrigation water use amount, which
hinders its direct application in agricultural water resource management and the validation for hydrological simulations. This

470   limitation stems from the simplicity of our mathematical approach, which makes it challenging to derive flow variables (i.e.,
irrigation water) from stock measurements (i.e., soil moisture).

Nonetheless, the fact that SMAP has the potential to reveal irrigation event occurrences provides a starting point for various applications. For example, the occurrence of irrigation activities can vary annually depending on the local agricultural management or land use changes. Such information cannot be captured by the static irrigated area map but could be revealed

475   by SMAP. One promising direction is the development of quasi-real-time irrigation occurrence maps based on dynamic SMAP estimations to improve the realism of current hydrological monitoring. Another direction is to incorporate machine learning tools to establish the relationship between monthly SMAP irrigation signals and limited observed irrigation water use amount data. By extending the relationship, it is promising to obtain water use amount data in observation-scarce regions.

Data availability

480   SMAP L3_E and L4 products are freely accessible via NASA Earthdata portal (http://earthdata.nasa.gov/). The Global Map of Irrigation Areas can be obtained through the FAO website (Geospatial Information). Irrigation water use estimates are available from https://doi.org/10.1029/2021WR031382 (Zhang and Long., 2021).

Author contributions

H. X. and Q. H. designed the study and wrote the original draft. R. R. proposed the research idea and contributed to manuscript

485   revision. N. H. and T. O. critically reviewed and edited the manuscript. All authors discussed experiments and results, provided substantial feedback, and approved the final version of the manuscript.

Competing interests

The authors declare that they have no conflict of interest.

Acknowledgements

495   for providing access to the CONUS irrigation water use data. The authors also acknowledge the invaluable assistance from the

NASA SMAP science team.

References

Alfieri, L., Avanzi, F., Delogu, F., Gabellani, S., Bruno, G., Campo, L., Libertino, A., Massari, C., Tarpanelli, A., Rains, D.,
Miralles, D.G., Quast, R., Vreugdenhil, M., Wu, H., Brocca, L., 2022. High-resolution satellite products improve
500   hydrological modeling in northern Italy. Hydrol. Earth Syst. Sci. 26, 3921–3939. https://doi.org/10.5194/hess-26-
3921-2022

Barre, H.M.J.P., Duesmann, B., Kerr, Y.H., 2008. SMOS: The Mission and the System. IEEE Trans. Geosci. Remote Sens.
46, 587–593. https://doi.org/10.1109/TGRS.2008.916264

Bastiaanssen, W.G.M., Cheema, M.J.M., Immerzeel, W.W., Miltenburg, I.J., Pelgrum, H., 2012. Surface energy balance and
505   actual evapotranspiration of the transboundary Indus Basin estimated from satellite measurements and the ETLook
model. Water Resour. Res. 48, 2011WR010482. https://doi.org/10.1029/2011WR010482

Brocca, L., Tarpanelli, A., Filippucci, P., Dorigo, W., Zaussinger, F., Gruber, A., Fernández-Prieto, D., 2018. How much
water is used for irrigation? A new approach exploiting coarse resolution satellite soil moisture products. Int. J.
Appl. Earth Obs. Geoinformation 73, 752–766. https://doi.org/10.1016/j.jag.2018.08.023

510   Colliander, A., Reichle, R.H., Crow, W.T., Cosh, M.H., Chen, F., Chan, S., Das, N.N., Bindlish, R., Chaubell, J., Kim, S.,
Liu, Q., O'Neill, P.E., Dunbar, R.S., Dang, L.B., Kimball, J.S., Jackson, T.J., Al-Jassar, H.K., Asanuma, J.,
Bhattacharya, B.K., Berg, A.A., Bosch, D.D., Bourgeau-Chavez, L., Caldwell, T., Calvet, J.-C., Collins, C.H.,
Jensen, K.H., Livingston, S., Lopez-Baeza, E., Martinez-Fernandez, J., McNairn, H., Moghaddam, M., Montzka,
C., Notarnicola, C., Pellarin, T., Greimeister-Pfeil, I., Pulliainen, J., Ramos, J.Gpe., Seyfried, M., Starks, P.J., Su, Z.,
515   Van Der Velde, R., Zeng, Y., Thibeault, M., Vreugdenhil, M., Walker, J.P., Zribi, M., Entekhabi, D., Yueh, S.H.,
2022. Validation of Soil Moisture Data Products From the NASA SMAP Mission. IEEE J. Sel. Top. Appl. Earth
Obs. Remote Sens. 15, 364–392. https://doi.org/10.1109/JSTARS.2021.3124743

Condon, L.E., Kollet, S., Bierkens, M.F.P., Fogg, G.E., Maxwell, R.M., Hill, M.C., Fransen, H.H., Verhoef, A., Van Loon,
A.F., Sulis, M., Abesser, C., 2021. Global Groundwater Modeling and Monitoring: Opportunities and Challenges.
520   Water Resour. Res. 57, e2020WR029500. https://doi.org/10.1029/2020WR029500

De Lannoy, G.J.M., Reichle, R.H., 2016. Global Assimilation of Multiangle and Multipolarization SMOS Brightness
Temperature Observations into the GEOS-5 Catchment Land Surface Model for Soil Moisture Estimation. J.
Hydrometeorol. 17, 669–691. https://doi.org/10.1175/JHM-D-15-0037.1

Dorigo, W., Himmelbauer, I., Aberer, D., Schremmer, L., Petrakovic, I., Zappa, L., Preimesberger, W., Xaver, A., Annor, F.,
525   Ardö, J., Baldocchi, D., Bitelli, M., Blöschl, G., Bogena, H., Brocca, L., Calvet, J.-C., Camarero, J.J., Capello, G.,
Choi, M., Cosh, M.C., Van De Giesen, N., Hajdu, I., Ikonen, J., Jensen, K.H., Kanniah, K.D., De Kat, I.,
Kirchengast, G., Kumar Rai, P., Kyrouac, J., Larson, K., Liu, S., Loew, A., Moghaddam, M., Martínez Fernández,
J., Mattar Bader, C., Morbidelli, R., Musial, J.P., Osenga, E., Palecki, M.A., Pellarin, T., Petropoulos, G.P., Pfeil, I.,
Powers, J., Robock, A., Rüdiger, C., Rummel, U., Strobel, M., Su, Z., Sullivan, R., Tagesson, T., Varlagin, A.,
530   Vreugdenhil, M., Walker, J., Wen, J., Wenger, F., Wigneron, J.P., Woods, M., Yang, K., Zeng, Y., Zhang, X., Zreda,
M., Dietrich, S., Gruber, A., Van Oevelen, P., Wagner, W., Scipal, K., Drusch, M., Sabia, R., 2021. The International
Soil Moisture Network: serving Earth system science for over a decade. Hydrol. Earth Syst. Sci. 25, 5749–5804.
https://doi.org/10.5194/hess-25-5749-2021

Droogers, P., Immerzeel, W.W., Lorite, I.J., 2010. Estimating actual irrigation application by remotely sensed
535   evapotranspiration observations. Agric. Water Manag. 97, 1351–1359. https://doi.org/10.1016/j.agwat.2010.03.017

Entekhabi, D., Njoku, E.G., O'Neill, P.E., Kellogg, K.H., Crow, W.T., Edelstein, W.N., Entin, J.K., Goodman, S.D., Jackson,

T.J., Johnson, J., Kimball, J., Piepmeier, J.R., Koster, R.D., Martin, N., McDonald, K.C., Moghaddam, M., Moran, S., Reichle, R., Shi, J.C., Spencer, M.W., Thurman, S.W., Tsang, L., Van Zyl, J., 2010. The Soil Moisture Active Passive (SMAP) Mission. Proc. IEEE 98, 704–716. https://doi.org/10.1109/JPROC.2010.2043918

540   Fang, K., Pan, M., Shen, C., 2019. The value of SMAP for long-term soil moisture estimation with the help of deep learning. IEEE Trans. Geosci. Remote Sens. 57, 2221–2233. https://doi.org/10.1109/TGRS.2018.2872131

FAO, UN Water, 2021. Progress on Level of Water Stress. Global status and acceleration needs for SDG Indicator 6.4.2, 2021. Rome. https://doi.org/10.4060/cb6241en

Faunt, C.C., 2009. Groundwater availability of the Central Valley aquifer, California, Professional Paper. U.S. Geological
545   Survey, Reston, VA.

Feldman, A.F., Short Gianotti, D.J., Dong, J., Akbar, R., Crow, W.T., McColl, K.A., Konings, A.G., Nippert, J.B., Tumber-Dávila, S.J., Holbrook, N.M., Rockwell, F.E., Scott, R.L., Reichle, R.H., Chatterjee, A., Joiner, J., Poulter, B., Entekhabi, D., 2023. Remotely sensed soil moisture can capture dynamics relevant to plant water uptake. Water Resour. Res. 59, e2022WR033814. https://doi.org/10.1029/2022WR033814

550   Foster, T., Mieno, T., Brozović, N., 2020. Satellite-based monitoring of irrigation water use: assessing measurement errors and their implications for agricultural water management policy. Water Resour. Res. 56, e2020WR028378. https://doi.org/10.1029/2020WR028378

Gowda, P.H., Chavez, J.L., Colaizzi, P.D., Evett, S.R., Howell, T.A., Tolk, J.A., 2008. ET mapping for agricultural water management: present status and challenges. Irrig. Sci. 26, 223–237. https://doi.org/10.1007/s00271-007-0088-6

555   Guillaumot, L., Smilovic, M., Burek, P., De Bruijn, J., Greve, P., Kahil, T., Wada, Y., 2022. Coupling a large-scale hydrological model (CWatM v1.1) with a high-resolution groundwater flow model (MODFLOW 6) to assess the impact of irrigation at regional scale. Geosci. Model Dev. 15, 7099–7120. https://doi.org/10.5194/gmd-15-7099-2022

Hanasaki, N., Kanae, S., Oki, T., Masuda, K., Motoya, K., Shirakawa, N., Shen, Y., Tanaka, K., 2008. An integrated model
560   for the assessment of global water resources – Part 1: Model description and input meteorological forcing. Hydrol. Earth Syst. Sci. 12, 1007–1025. https://doi.org/10.5194/hess-12-1007-2008

Hanasaki, N., Matsuda, H., Fujiwara, M., Hirabayashi, Y., Seto, S., Kanae, S., Oki, T., 2022. Toward hyper-resolution global hydrological models including human activities: application to Kyushu island, Japan. Hydrol. Earth Syst. Sci. 26, 1953–1975. https://doi.org/10.5194/hess-26-1953-2022

565   Ihuoma, S.O., Madramootoo, C.A., Kalacska, M., 2021. Integration of satellite imagery and in situ soil moisture data for estimating irrigation water requirements. Int. J. Appl. Earth Obs. Geoinformation 102, 102396. https://doi.org/10.1016/j.jag.2021.102396

Jalilvand, E., Abolafia-Rosenzweig, R., Tajrishy, M., Das, N., 2021. Evaluation of SMAP/Sentinel 1 high-resolution soil moisture data to detect irrigation over agricultural domain. IEEE J. Sel. Top. Appl. Earth Obs. Remote Sens. 14,
570   10733–10747. https://doi.org/10.1109/JSTARS.2021.3119228

Jalilvand, E., Abolafia-Rosenzweig, R., Tajrishy, M., Kumar, S.V., Mohammadi, M.R., Das, N.N., 2023. Is it possible to quantify irrigation water‐use by assimilating a high‐resolution satellite soil moisture product? Water Resour. Res. 59, e2022WR033342. https://doi.org/10.1029/2022WR033342

Jalilvand, E., Tajrishy, M., Ghazi Zadeh Hashemi, S.A., Brocca, L., 2019. Quantification of irrigation water using remote
575   sensing of soil moisture in a semi-arid region. Remote Sens. Environ. 231, 111226. https://doi.org/10.1016/j.rse.2019.111226

Jonard, F., Feldman, A.F., Short Gianotti, D.J., Entekhabi, D., 2022. Observed water and light limitation across global ecosystems. Biogeosciences 19, 5575–5590. https://doi.org/10.5194/bg-19-5575-2022

Koster, R.D., Suarez, M.J., Ducharne, A., Stieglitz, M., Kumar, P., 2000. A catchment-based approach to modeling land
580   surface processes in a general circulation model: 1. Model structure. J. Geophys. Res. Atmospheres 105, 24809–24822. https://doi.org/10.1029/2000JD900327

Kottek, M., Grieser, J., Beck, C., Rudolf, B., Rubel, F., 2006. World map of the Köppen-Geiger climate classification

updated. Meteorol. Z. 15, 259–263. https://doi.org/10.1127/0941-2948/2006/0130

Lawston, P.M., Santanello, J.A., Kumar, S.V., 2017. Irrigation signals detected from SMAP soil moisture retrievals.
585   Geophys. Res. Lett. 44. https://doi.org/10.1002/2017GL075733

Liu, K., Bo, Y., Li, X., Wang, S., Zhou, G., 2024. Uncovering current and future variations of irrigation water use across
China using machine learning. Earth's Future. 12, e2023EF003562. https://doi.org/10.1029/2023EF003562

Ma, Y., Liu, S., Song, L., Xu, Z., Liu, Y., Xu, T., Zhu, Z., 2018. Estimation of daily evapotranspiration and irrigation water
efficiency at a Landsat-like scale for an arid irrigation area using multi-source remote sensing data. Remote Sens.
590   Environ. 216, 715–734. https://doi.org/10.1016/j.rse.2018.07.019

McColl, K.A., Alemohammad, S.H., Akbar, R., Konings, A.G., Yueh, S., Entekhabi, D., 2017. The global distribution and
dynamics of surface soil moisture. Nat. Geosci. 10, 100–104. https://doi.org/10.1038/ngeo2868

McDermid, S., Nocco, M., Lawston-Parker, P., Keune, J., Pokhrel, Y., Jain, M., Jägermeyr, J., Brocca, L., Massari, C., Jones,
A.D., Vahmani, P., Thiery, W., Yao, Y., Bell, A., Chen, L., Dorigo, W., Hanasaki, N., Jasechko, S., Lo, M.-H.,
595   Mahmood, R., Mishra, V., Mueller, N.D., Niyogi, D., Rabin, S.S., Sloat, L., Wada, Y., Zappa, L., Chen, F., Cook,
B.I., Kim, H., Lombardozzi, D., Polcher, J., Ryu, D., Santanello, J., Satoh, Y., Seneviratne, S., Singh, D., Yokohata,
T., 2023. Irrigation in the Earth system. Nat. Rev. Earth Environ. 4, 435–453. https://doi.org/10.1038/s43017-023-
00438-5

Melser, R., Coops, N.C., Derksen, C., 2024. Characterizing satellite-derived freeze/thaw regimes through spatial and
600   temporal clustering for the identification of growing season constraints on vegetation productivity. Remote Sens.
Environ. 309, 114210. https://doi.org/10.1016/j.rse.2024.114210

Müller Schmied, H., Cáceres, D., Eisner, S., Flörke, M., Herbert, C., Niemann, C., Peiris, T.A., Popat, E., Portmann, F.T.,
Reinecke, R., Schumacher, M., Shadkam, S., Telteu, C.-E., Trautmann, T., Döll, P., 2021. The global water
resources and use model WaterGAP v2.2d: model description and evaluation. Geosci. Model Dev. 14, 1037–1079.
605   https://doi.org/10.5194/gmd-14-1037-2021

Murray, E.M., 2018. Idaho water use, 2015 (Report No. 2018–3036), Fact Sheet. Reston, VA.
https://doi.org/10.3133/fs20183036

Njoku, E.G., Entekhabi, D., 1996. Passive microwave remote sensing of soil moisture. J. Hydrol. 184, 101–129.
https://doi.org/10.1016/0022-1694(95)02970-2

610   O'Neill, P., Chan, S., Bindlish, R., Chaubell, M., Colliander, A., Chen, F., Dunbar, S., Jackson, T., Cosh, M., Bongiovanni,
T., Walker, J., Wu, X., Berg, A., McNairn, H., Thibeault, M., Martínez, J., González-Zamora, Á., Lopez-Baeza, E.,
Jensen, K., Seyfried, M., Bosch, D., Starks, P., Collins, C.H., Prueger, J., Su, Z., Calvet, J., Crow, W., Kerr, Y.,
Yueh, S., Entekhabi, D., 2020. Soil Moisture Active Passive (SMAP) Project: calibration and validation for the
L2/3_SM_P Version 7 and L2/3_SM_P_E version 4 data products. Jet Propuls. Lab.

615   ONeill, P.E., Chan, S., Njoku, E.G., Jackson, T., Bindlish, R., Chaubell, M.J., Colliander, A., 2023. SMAP enhanced L3
radiometer global and polar grid daily 9 km EASE-Grid soil moisture, Version 6.
https://doi.org/10.5067/M20OXIZHY3RJ

Ozdogan, M., Yang, Y., Allez, G., Cervantes, C., 2010. Remote Sensing of Irrigated Agriculture: Opportunities and
Challenges. Remote Sens. 2, 2274–2304. https://doi.org/10.3390/rs2092274

620   Purdy, A.J., Fisher, J.B., Goulden, M.L., Colliander, A., Halverson, G., Tu, K., Famiglietti, J.S., 2018. SMAP soil moisture
improves global evapotranspiration. Remote Sens. Environ. 219, 1–14. https://doi.org/10.1016/j.rse.2018.09.023

Reichle, R.H., De Lannoy, G., Koster, R., Crow, W., Kimball, J., Liu, Q., Bechtold, M., 2022. SMAP L4 global 3-hourly 9
km EASE-Grid surface and root zone soil moisture geophysical data, Version 7.
https://doi.org/10.5067/EVKPQZ4AFC4D

625   Reichle, R.H., De Lannoy, G.J.M., Liu, Q., Ardizzone, J.V., Colliander, A., Conaty, A., Crow, W., Jackson, T.J., Jones, L.A.,
Kimball, J.S., Koster, R.D., Mahanama, S.P., Smith, E.B., Berg, A., Bircher, S., Bosch, D., Caldwell, T.G., Cosh,
M., González-Zamora, Á., Holifield Collins, C.D., Jensen, K.H., Livingston, S., Lopez-Baeza, E., Martínez-
Fernández, J., McNairn, H., Moghaddam, M., Pacheco, A., Pellarin, T., Prueger, J., Rowlandson, T., Seyfried, M.,

630 Starks, P., Su, Z., Thibeault, M., Van Der Velde, R., Walker, J., Wu, X., Zeng, Y., 2017a. Assessment of the SMAP
        Level-4 surface and root-zone soil moisture product using in situ measurements. J. Hydrometeorol. 18, 2621–2645.
        https://doi.org/10.1175/JHM-D-17-0063.1

Reichle, R.H., De Lannoy, G.J.M., Liu, Q., Koster, R.D., Kimball, J.S., Crow, W.T., Ardizzone, J.V., Chakraborty, P., Collins,
        D.W., Conaty, A.L., Girotto, M., Jones, L.A., Kolassa, J., Lievens, H., Lucchesi, R.A., Smith, E.B., 2017b. Global
        assessment of the SMAP Level-4 surface and root-zone soil moisture product using assimilation diagnostics. J.
635   Hydrometeorol. 18, 3217–3237. https://doi.org/10.1175/JHM-D-17-0130.1

Reichle, R.H., Liu, Q., Ardizzone, J.V., Bechtold, M., Crow, W.T., De Lannoy, G.J.M., Kimball, J.S., Koster, R.D., 2023a.
        Soil Moisture Active Passive (SMAP) project assessment report for version 7 of the L4_SM data product.
        NASA/TM-2023-104606 Vol. 64, 91 pp. https://gmao.gsfc.nasa.gov/pubs/

Reichle, R.H., Liu, Q., Ardizzone, J.V., Crow, W.T., De Lannoy, G.J.M., Kimball, J.S., Koster, R.D., 2023b. IMERG
640   precipitation improves the SMAP Level-4 soil moisture product. J. Hydrometeorol. 24, 1699–1723.
        https://doi.org/10.1175/JHM-D-23-0063.1

Reichle, R.H., Liu, Q., Koster, R.D., Crow, W.T., De Lannoy, G.J.M., Kimball, J.S., Ardizzone, J.V., Bosch, D., Colliander,
        A., Cosh, M., Kolassa, J., Mahanama, S.P., Prueger, J., Starks, P., Walker, J.P., 2019. Version 4 of the SMAP Level-
        4 soil moisture algorithm and data product. J. Adv. Model. Earth Syst. 11, 3106–3130.
645   https://doi.org/10.1029/2019MS001729

Ritchie, H., Roser, M., 2018. Water Use and Stress. Our World Data.

Sacks, W.J., Deryng, D., Foley, J.A., Ramankutty, N., 2010. Crop planting dates: an analysis of global patterns. Glob. Ecol.
        Biogeogr. 19, 607–620. https://doi.org/10.1111/j.1466-8238.2010.00551.x

Santos, C., Lorite, I.J., Tasumi, M., Allen, R.G., Fereres, E., 2008. Integrating satellite-based evapotranspiration with
650   simulation models for irrigation management at the scheme level. Irrig. Sci. 26, 277–288.
        https://doi.org/10.1007/s00271-007-0093-9

See, L., Gilliams, S., Conchedda, G., Degerickx, J., Van Tricht, K., Fritz, S., Lesiv, M., Laso Bayas, J.C., Rosero, J.,
        Tubiello, F.N., Szantoi, Z., 2023. Dynamic global-scale crop and irrigation monitoring. Nat. Food 4, 736–737.
        https://doi.org/10.1038/s43016-023-00841-7

655 Siebert, S., Henrich, V., Frenken, K., Burke, J., 2013. Global map of irrigation areas version 5.

Singh, V., Zhou, S., Ganie, Z., Valverde, B., Avila, L., Marchesan, E., Merotto, A., Zorrilla, G., Burgos, N., Norsworthy, J.,
        Bagavathiannan, M., 2017. Rice production in the Americas, in: Chauhan, B.S., Jabran, K., Mahajan, G., Rice
        Production Worldwide. Springer International Publishing, Cham, pp. 137–168. https://doi.org/10.1007/978-3-319-
        47516-5_6

660 Sorooshian, S., AghaKouchak, A., Li, J., 2014. Influence of irrigation on land hydrological processes over California. J.
        Geophys. Res. Atmospheres 119. https://doi.org/10.1002/2014JD022232

Soylu, M.E., Bras, R.L., 2024. Quantifying and valuing irrigation in energy and water limited agroecosystems. J. Hydrol. X
        22, 100169. https://doi.org/10.1016/j.hydroa.2023.100169

Sutanudjaja, E.H., Van Beek, R., Wanders, N., Wada, Y., Bosmans, J.H.C., Drost, N., Van Der Ent, R.J., De Graaf, I.E.M.,
665   Hoch, J.M., De Jong, K., Karssenberg, D., López López, P., Peßenteiner, S., Schmitz, O., Straatsma, M.W.,
        Vannametee, E., Wisser, D., Bierkens, M.F.P., 2018. PCR-GLOBWB 2: a 5 arcmin global hydrological and water
        resources model. Geosci. Model Dev. 11, 2429–2453. https://doi.org/10.5194/gmd-11-2429-2018

U.S. Department of Agriculture, National Agricultural Statistics Service, 2024. Irrigation and Water Management Survey.
        https://www.nass.usda.gov/Surveys/Guide_to_NASS_Surveys/Farm_and_Ranch_Irrigation/

670 Wada, Y., Wisser, D., Eisner, S., Flörke, M., Gerten, D., Haddeland, I., Hanasaki, N., Masaki, Y., Portmann, F.T., Stacke, T.,
        Tessler, Z., Schewe, J., 2013. Multimodel projections and uncertainties of irrigation water demand under climate
        change. Geophys. Res. Lett. 40, 4626–4632. https://doi.org/10.1002/grl.50686

Wei, S., Xu, T., Niu, G.-Y., Zeng, R., 2022. Estimating irrigation water consumption using machine learning and remote
        sensing data in Kansas High Plains. Remote Sens. 14, 3004. https://doi.org/10.3390/rs14133004

675   Wong, A.J., Jin, Y., Medellín-Azuara, J., Paw U, K.T., Kent, E.R., Clay, J.M., Gao, F., Fisher, J.B., Rivera, G., Lee, C.M.,
         Hemes, K.S., Eichelmann, E., Baldocchi, D.D., Hook, S.J., 2021. Multiscale assessment of agricultural
         consumptive water use in California's Central Valley. Water Resour. Res. 57, e2020WR028876.
         https://doi.org/10.1029/2020WR028876

         Yang, Z., Dominguez, F., Zeng, X., Hu, H., Gupta, H., Yang, B., 2017. Impact of irrigation over the California Central Valley
680   on regional climate. J. Hydrometeorol. 18, 1341–1357. https://doi.org/10.1175/JHM-D-16-0158.1

         Zaussinger, F., Dorigo, W., Gruber, A., Tarpanelli, A., Filippucci, P., Brocca, L., 2019. Estimating irrigation water use over
         the contiguous United States by combining satellite and reanalysis soil moisture data. Hydrol. Earth Syst. Sci. 23,
         897–923. https://doi.org/10.5194/hess-23-897-2019

         Zhang, C., Long, D., 2021. Estimating spatially explicit irrigation water use based on remotely sensed evapotranspiration
685   and modeled root zone soil moisture. Water Resour. Res. 57, e2021WR031382.
         https://doi.org/10.1029/2021WR031382

         Zhang, K., Kimball, J.S., Running, S.W., 2016. A review of remote sensing based actual evapotranspiration estimation.
         WIREs Water 3, 834–853. https://doi.org/10.1002/wat2.1168

         Zhang, K., Li, X., Zheng, D., Zhang, L., Zhu, G., 2022. Estimation of global irrigation water use by the integration of
690   multiple satellite observations. Water Resour. Res. 58, e2021WR030031. https://doi.org/10.1029/2021WR030031